DOI: 10.1002/cmdc.201100094

Discovery, Structure–Activity Relationship Studies, and Crystal Structure of Nonpeptide Inhibitors Bound to the Shank3 PDZ Domain

Jörn Saupe,[b, c] Yvette Roske,[d] Christian Schillinger,[b] Nestor Kamdem,[b, c] Silke Radetzki,[b] Anne Diehl,[b] Hartmut Oschkinat,[b, c] Gerd Krause,[b] Udo Heinemann,[c, d] and Jörg Rademann*[a, b]

Shank is the central scaffolding protein of the postsynaptic density (PSD) protein complex found in cells of the central nervous system. Cellular studies indicate a prominent role of the protein in the organization of the PSD, in the development of neuronal morphology, in neuronal signaling, and in synaptic plasticity, thus linking Shank functions to the molecular basis of learning and memory. Mutations in the Shank gene have been found in several neuronal disorders including mental retardation, typical autism, and Asperger syndrome. Shank is linked to the PSD complex via its PDZ domain that binds to the C-terminus of guanylate-kinase-associated protein (GKAP). Here, small-molecule inhibitors of Shank3 PDZ domain are developed. A fluorescence polarization assay based on an identified high-affinity peptide is established, and tetrahydroquinoline carboxylates are identified as inhibitors of this protein–protein interaction. Chemical synthesis via a hetero-Diels–Alder strategy is employed for hit optimization, and structure–activity relationship studies are performed. Best hits possess K_i values in the 10 μM range, and binding to the PDZ domain is confirmed by $^1H,^{15}N$ HSQC NMR experiments. One of the hits crystallizes with the Shank3 PDZ domain. The structure, analyzed at a resolution of 1.85 Å, reveals details of the binding mode. Finally, binding to PDZ domains of PSD-95, syntrophin, and DVL3 was studied using $^1H,^{15}N$ HSQC NMR spectroscopy.

Introduction

Most events in signal transduction of cells and organisms are mediated by protein complexes, large assemblies of proteins that arise from specific protein–protein interactions (PPIs). Interference with PPIs can be a powerful strategy to modulate cellular signals; however, the development of small molecules interfering specifically with single PPI domains has been a tremendous challenge for medicinal chemistry and succeeded only in few instances until now.[1,2]

PDZ domains which recognize the C-terminus of their target polypeptides form a large and widespread family of PPI domains.[3] Occasionally, binding to internal target sequences without disrupting the structure of their targets has been reported as well.[4,5] The C-terminal carboxylate usually interacts with several backbone amides of a loop region within the PDZ domain, the so-called carboxylate-binding loop.[6] PDZ domains have been named according to the first three reported examples of this protein class, namely the proteins PSD-95, DLG, and ZO-1.[7] PDZ domains are considered difficult to target with small molecules.[8,9] However, there are small-molecule inhibitors known of these PPI domains, for example, for the PDZ domains of Disheveled[10,11] and protein interacting with C kinase-1 (PICK1)[12], with affinities of roughly 10 μM.

A prominent example for a protein network, organized mainly by PDZ domain interactions, is the postsynaptic density (PSD) in the cells of the central nervous system.[13,14] In the PSD, clusters of glutamate receptors are organized via PDZ interactions mainly to the proteins PSD-95, PICK1, and glutamate receptor-interacting protein (GRIP) (Figure 1).

The central scaffolding protein of the postsynaptic density is Shank. It appears in three isoforms, Shank 1–3, showing pairwise amino acid sequence identities of 63–87 %.[15] This protein interlinks clusters of glutamate receptors of the metabotropic as well as the ionotropic type including the *N*-methyl-D-aspartate (NMDA) and α-amino-3-hydroxy-5-methyl-4-isoxazole propionate (AMPA) receptors in the PSD.[16] Shank is attached to the PSD via its PDZ domain recognizing the C-terminus of the

[a] *Prof. Dr. J. Rademann*
Institute of Pharmacy, Leipzig University
Brüderstr. 34, 04103 Leipzig (Germany)
Fax: (+49) 341-9737-709
E-mail: rademann@uni-leipzig.de

[b] *J. Saupe, C. Schillinger, N. Kamdem, Dr. S. Radetzki, Dr. A. Diehl, Prof. Dr. H. Oschkinat, Dr. G. Krause, Prof. Dr. J. Rademann*
Leibniz-Institut für Molekulare Pharmakologie (FMP)
Robert-Rössle-Str. 10, 13125 Berlin (Germany)

[c] *J. Saupe, N. Kamdem, Prof. Dr. H. Oschkinat, Prof. Dr. U. Heinemann*
Institute of Chemistry and Biochemistry
Freie Universität Berlin (Germany)
Takustr. 3, 14195 Berlin (Germany)

[d] *Dr. Y. Roske, Prof. Dr. U. Heinemann*
Max Delbrück Center for Molecular Medicine (MDC)
Robert-Rössle-Str. 10, 13125 Berlin (Germany)

Supporting information for this article is available on the WWW under http://dx.doi.org/10.1002/cmdc.201100094.

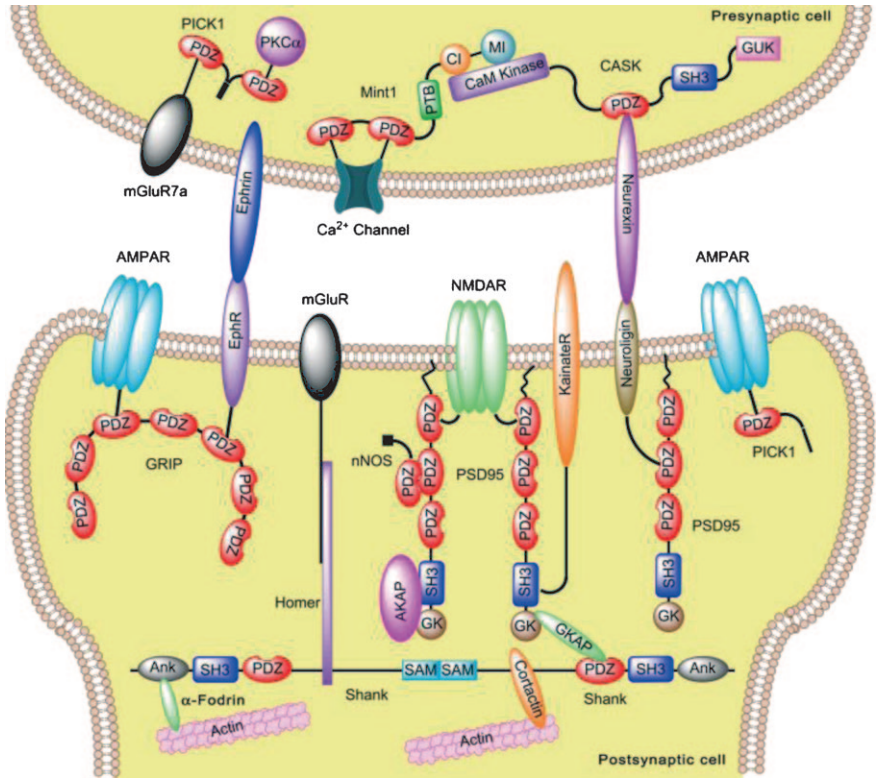

Figure 1. PDZ domain-mediated organization of macromolecular complexes in neurons. On the postsynaptic element, PSD-95 uses its PDZ domains to bind to the PDZ domain of neuronal nitric oxide synthase (nNOS), the C-termini of the NMDA receptor, and neuroligin. The SH3 domain binds the kainate receptor. An N-terminal palmitate group (wavy line) attaches PSD-95 to the postsynaptic membrane. GKAP binds to the guanylate kinase (GK) domain of PSD-95 and connects it with the PDZ domain of Shank. Shank, as central scaffolding protein, also anchors the mGluRs along with the bridge protein Homer. The SAM domain is responsible for the multimerization of Shank. Cortactin and α-fodrin link Shank and the different types of bound receptors directly to the cytoskeleton. Two additional proteins bind to the AMPA receptor via its PDZ domains: one is the seven PDZ domains-containing GRIP, which also binds the ephrin receptor 9 (EphR9) through a PDZ domain, and the other is PICK. The cell adhesion molecules neurexin and neuroligin form the intercellular junction. Neurexin interacts with the calcium/calmodulin-dependent serine protein kinase (CASK) PDZ domain on the presynaptic side. CASK also interacts with the N-terminus of Mint1, which binds via its two PDZ domains to N-type Ca^{2+} channels. The C-terminus of mGluR7a and the catalytic subunit of protein kinase Cα (PKCα) interact with the PDZ domain of PICK1.

protein GKAP[17] and through the bridging protein Homer binding to the proline-rich region of Shank.[13] A direct interaction of metabotropic glutamate receptors (mGluRs)[18,19] and somatostatin receptor subtype 2 (SSTR2)[20,21] with the Shank PDZ domain was discussed as well. In addition, there are hints suggesting that the Src-homology 3 (SH3) domain of Shank binds to GRIP.[15] On the other end, Shank anchors the entire PSD protein cluster to the actin cytoskeleton via cortactin binding to the proline-rich region[17] and α-fodrin binding to the ankyrin repeats (Ank),[16] as illustrated in Figure 1. The oligomerization of Shank is mediated by its sterile alpha motif (SAM) domain.[22] Cellular studies have indicated a dominant role of the protein in the organization of the PSD, in the development of neuronal morphology, in neuronal signaling, and in synaptic plasticity,[15] thereby linking Shank functionally to the molecular basis of learning and memory.[23,24] Mutations in the *Shank* gene have been found in several neuronal disorders including mental retardation, typical autism, and Asperger syndrome.[25,26] Genetic deletion of the C-terminus of the protein dendrite arborization and synapse maturation 1 (Dasm1), which was shown to interact strongly and selectively with the Shank PDZ domain, had a strong inhibitory effect on hippocampal neuronal maturation.[27] In a single report, a significant role of the Shank3 PDZ domain in signaling of the Ret9 receptor has been described.[28]

For these reasons, we selected the Shank3 PDZ domain as a biologically attractive target for the development of small-molecule PDZ ligands. Shank3 PDZ inhibitors could be useful to investigate the functional significance of Shank3 PDZ interactions for the overall function of Shank3 and the organization of the PSD, and could be of value for the functional modulation of synaptic functions including plasticity in the future.

For screening of Shank3 PDZ interactions, a homogeneous binding assay based on fluorescence polarization (FP) was developed. A high-affinity peptide was selected from a small collection of fluorescently labeled peptides derived from the C-termini of putative protein interaction partners of the Shank PDZ domain. This peptide, which could act as an inhibitor of the Shank3 PDZ domain by itself, was used to find small-molecule inhibitors; this strategy was considered attractive due to the known limitations of peptides in living systems. Deficiencies ascribed to the molecular weight and polarity of peptides include: a) rapid metabolism by proteases in the gastrointestinal tract, blood, and numerous tissues; b) rapid excretion by kidney and liver; and c) poor transport through the blood-brain barrier and cell membranes or even from the gastrointestinal tract to the blood.[29] Problems passing the cell membrane can be avoided using peptidic, cell-permeable attachments such as penetratin.[30] In general, however, nonpeptide inhibitors possess several advantageous properties, among them a higher stability with respect to biodegradation.

Primary hits from a screen of the ChemBioNet library[31] were used as starting points for the synthesis of a number of derivatives, which provided detailed structure–activity relations of the hit. Validated hits were confirmed by NMR spectroscopy with ^{15}N-labeled Shank3 PDZ, indicating binding to the protein through significant shifts of several amide protons. One of these hit compounds was co-crystallized with the Shank3 PDZ domain to determine the binding mode. Finally, binding stud-

ies employing NMR spectroscopy for detection of protein binding were conducted with respect to five PDZ domains including DVL3, syntrophin, and the three PDZ domains of PSD-95.

Results and Discussion

Shank3 PDZ expression

The correct definition of protein domains and their boundaries is an essential prerequisite for the production of soluble, recombinant proteins. Thus, PDZ domains were identified by using the alignment algorithm SMART (http://smart.embl.de)[32] and annotated using UniProt entry Q4ACU6 (figure S1, Supporting Information). The Shank3 construct was designed in accordance with the reported successful construct for Shank1 (PDB: 1Q3P).[33]

For comparison, an N- and C-terminally truncated Shank3 PDZ construct based on the UniProt annotation (Shank3-Q4ACU6) was expressed; however, expression of this construct yielded insoluble protein (data not shown). By contrast, expression of the designed extended Shank3 PDZ construct (Figure S1) in *E. coli* resulted in soluble protein with a yield of 1000 mg L^{-1} on auto-inducing and 400 mg L^{-1} on minimal medium. Clearly, extension of the annotated core domain according to secondary structure predictions or, in ideal cases, to soluble homologous constructs was essential to synthesize soluble protein. Efficient protein production relied on the use of the auto-inducing growth medium according to Studier[34] and enabled subsequent high-throughput screening (HTS).

Assay development and screening

Similar to an already known FP probe derived from the C-terminus of GKAP,[35] the hexapeptide **3** containing an amino acid sequence of GKAP was used. Peptide **3** was selected from a small collection of six fluorophore-labeled peptides (**1**–**6**, table S1, Supporting Information) with sequences derived from the C-termini of native interaction partners. The hexapeptide **3** (CF-EAQTRL-OH) possessed a K_d of 430 nM. Replacement of peptide **3** by the unlabeled peptide **7** (Ac-EAQTRL-OH) was investigated in a competition assay. The IC_{50} value for **7** was determined and converted into the K_i value ($K_i = 495$ nM) according to the procedure of Nikolovska-Coleska and co-workers.[36] The K_d value of the fluorescein-labeled peptide **3** (430 nM) was similar to the K_i value of the acetylated peptide **7** (495 nM), as expected for an interaction that is not modified significantly by an N-terminal label.

To determine the applicability of the assay for HTS, the Z' factor was determined.[37] Therefore, bound and free states were measured 192 times each to calculate the fluorescence polarization values and standard deviations for each state. The Z' factor was calculated to 0.71, thus showing the applicability for HTS.

Subsequently, the ChemBioNet library,[31] which we had recently assembled based on substructure composition, was assayed employing the FP binding assay for the Shank3 PDZ domain. Screening was accomplished in a 384-well format using a compound concentration of 10 μM. A compound was considered active if the FP was decreased by at least 15% relative to on-plate controls. The screening resulted in 27 primary hit compounds, of which 14 compounds were discarded due to autofluorescence that interfered with the assay read-out. Compounds were considered autofluorescent when a 10% increase in total fluorescence intensity was observed with respect to on-plate controls. The remaining 13 hit compounds were tested in a concentration-dependent manner. For only two of them (**34** and **35**, Table S2, Figure 3), IC_{50} values below 250 μM were determined. Both compounds contained tetrahydroquinoline carboxylate **8** as a core structure (Figure 2).

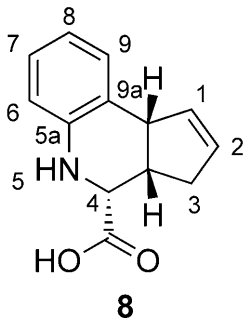

8

Figure 2. Active core structure **8** derived from screening the ChemBioNet library.

Chemistry

Retrosynthetic analysis of the hit scaffold, hetero-tricycle **8**, suggested the application of an aza-Diels–Alder reaction under Lewis acid catalysis for its preparation (Scheme 1). Condensation of anilines (**9**–**18**) with glyoxylic acid ester **19** was expected to provide imine intermediates in situ that should react

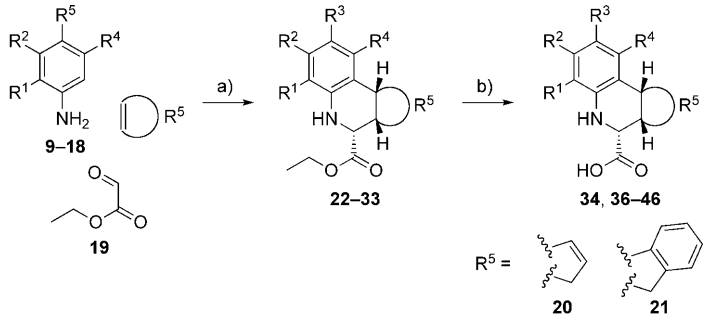

	R^1	R^2	R^3	R^4
9	OH	H	Cl	NO_2
10	CO_2Me	H	H	NO_2
11	H	H	CO_2Me	H
12	H	H	$CONH_2$	H
13	CO_2Me	H	H	H
14	H	H	H	H
15	OH	H	H	H
16	H	H	Br	H
17	OH	H	H	NO_2
18	H	H	H	NO_2

	R^1	R^2	R^3	R^4	R^5
22	OH	H	Cl	NO_2	**20**
23	CO_2Me	H	H	NO_2	**20**
24	H	H	CO_2Me	H	**20**
25	H	H	$CONH_2$	H	**20**
26	CO_2Me	H	H	H	**20**
27	H	H	H	H	**20**
28	OH	H	H	H	**20**
29	H	H	Br	H	**20**
30	OH	H	H	NO_2	**20**
31	H	NO_2	H	H	**20**
32	H	H	H	NO_2	**20**
33	OH	H	Cl	NO_2	**21**

Scheme 1. Synthesis of tetrahydroquinoline carboxylates: a) $Cu(OTf)_2$, MeCN, molecular sieves (4 Å), RT, 6 h; b) aq. LiOH/THF or aq. LiOH/MeOH, RT, 2 h.

Table 1. Optimization of the conditions for the synthesis of tetrahydrocyclopenta[*c*]quinoline carboxylates.

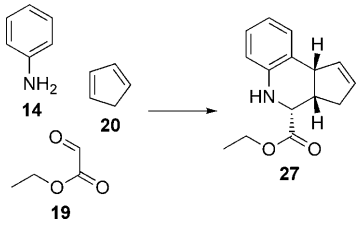

Lewis acid	mol%	solvent	yield[a]
$Cu(OTf)_2$	0	MeCN	0
$Cu(OTf)_2$	5	MeCN	48
$Cu(OTf)_2$	10	MeCN	43
$Cu(OTf)_2$	25	MeCN	34
$Cu(OTf)_2$	5	toluene	41
$Cu(OTf)_2$	5	$CHCl_3$	49
$Sc(OTf)_3$	5	MeCN	40
$BF_3{\cdot}OEt_2$	5	MeCN	45
$ZnCl_2$	5	MeCN	45
MgI_2	5	MeCN	24
$TiCl_4$	5	MeCN	18

[a] Isolated yield after flash chromatography.

subsequently as heterodienes with electron-rich dienophiles, i.e., freshly prepared cyclopentadiene (**20**) or indene (**21**), furnishing the desired tetrahydroquinoline carboxylate ester derivatives (**22**–**33**). Finally, saponification should yield the tetrahydrocyclopenta[*c*]- and tetrahydroindeno[2,1-*c*]quinoline carboxylates (**34**, **36**–**46**; Scheme 1).[38]

The reaction conditions were optimized for the synthesis of **27** using different Lewis acids and solvents in presence of molecular sieves (4 Å) (Table 1). In general, all Lewis acids tested were able to catalyze the cycloaddition. Soft to borderline Lewis acids like $Cu(OTf)_2$ or $ZnCl_2$ were superior catalysts, whereas hard Lewis acids like $TiCl_4$ or MgI_2 catalyzed the reaction with lower efficiency. Boron trifluoride, being a hard Lewis acid, was an exception as it catalyzed the reaction as efficiently as $ZnCl_2$. No product was formed in the absence of a Lewis acid catalyst. The most potent Lewis acid, copper(II) triflate (Table 1), was used to determine the influence of different solvents and amounts of the catalyst. Compound **27** was obtained in similar yields with all tested solvents (Table 1). Only a slight decrease in yield was observed for toluene, the least polar solvent used. Due to its ability to dissolve Lewis acids, acetonitrile was selected for synthesis of tetrahydroquinoline derivatives; in addition, the amount of Lewis acid was limited to 5 mol% $Cu(OTf)_2$, as higher concentrations led to decreased yields (Table 1).

Most anilines used for the synthesis of tetrahydroquinolines **34**–**46** were purchased from commercial suppliers. Only anilines **9** and **10** were synthesized according to literature procedures.[39,40] The synthesized compounds **22**–**33** were obtained in 14–81% yield depending on the substituents of the aniline; isolated yields were similar to those previously reported.[41] During the synthesis of **24**, the byproduct **50** (Scheme 2) was isolated in a yield of 11%. It was generated by amide formation of the tetrahydrocyclopenta[*c*]quinoline carboxylate with the aniline derivative. In the other reactions, however, no byproducts were isolated.

As previously described,[42] the cycloaddition occurred regio- and diastereoselectively. Analysis by NMR spectroscopy indicated that the orientation of the ethyl ester was *cis* with respect to the cyclopentene ring, and only 3*H* isomers were formed as shown in the crystal structure of **36** in complex with the Shank3 PDZ domain (vide infra). Extended efforts to establish an enantioselective synthesis, for example, by the use of chiral Lewis acids, failed.

Selective deprotection of the diacid ester **24** to **51** and further modification by anhydride activation resulted in the protected amide **52** and alcohol **53** (Scheme 2), which were both saponified to furnish **54** and **55**, respectively. Compound **35** was synthesized starting from deprotected **39** by addition of 2-nitrobenzenesulfenyl chloride (**63**) in dry acetonitrile. The reaction yielded 87% of **35** after column chromatography (Scheme 3). The remaining compounds used (i.e., **56**–**62**) were purchased from ChemDiv Inc. (San Diego, CA, USA) or were already part of in-house libraries (for a complete list, see Supporting Information table S2).

Testing of the tetrahydroquinoline derivatives revealed four compounds with K_i values below 250 μM (Figure 3). Whereas the K_i values of **34**–**36** were in the same range (K_i between

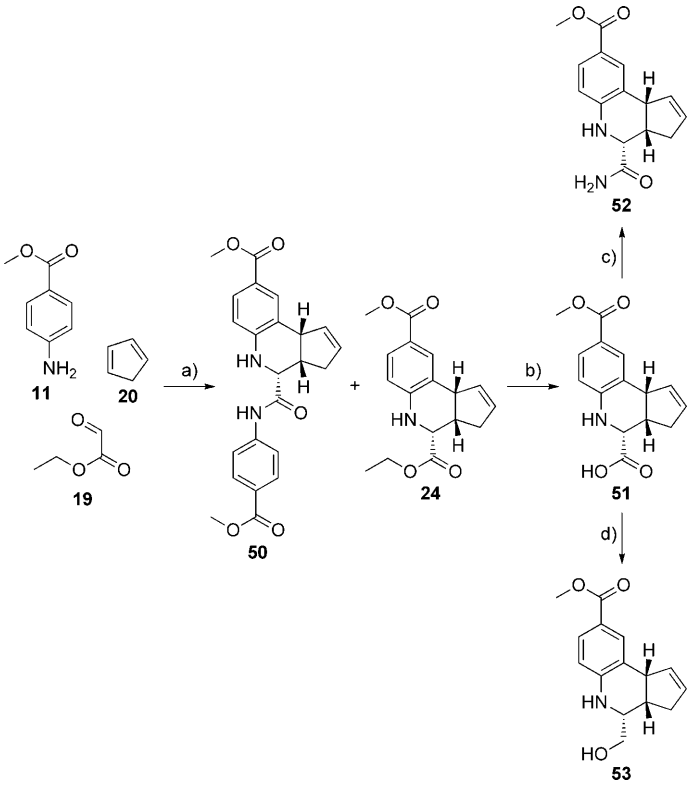

Scheme 2. Synthesis of compound **24**, protected amide **52**, alcohol **53**, and isolated byproduct **50**: a) $Cu(OTf)_2$, molecular sieves (4 Å), MeCN, RT, 6 h; b) 0.1 M aq. NaOH/THF, RT, 2 h; c) Boc_2O, NH_4HCO_3, pyridine, dioxane, RT, 18 h; d) isopropyl chloroformate, *N*-methylmorpholine, $NaBH_4$, 1,2-dimethoxyethane, −15 °C, 10 min.

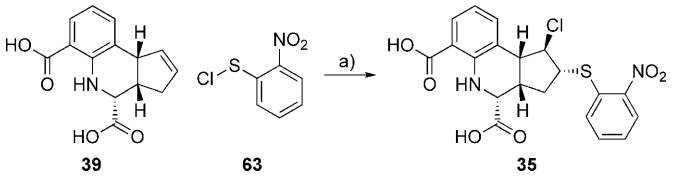

Scheme 3. Synthesis of compound **35** via sulfenyl chloride addition: a) MeCN, RT, 0.5 h.

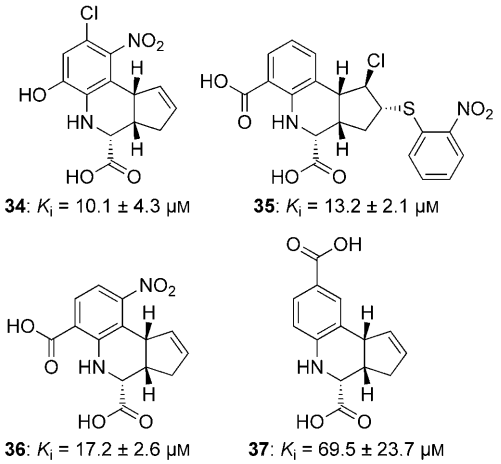

Figure 3. Structures and K_i values of active compounds **34**–**37**.

10.1 and 17.2 μM), **37** had a somewhat higher K_i value of 69.5 μM (Figure 3). All other compounds (**38**–**46**, **51**, and **54**–**62**) showed K_i values above 250 μM and were considered inactive (Table S2).

Validation of active compounds and qualitative binding studies with PDZ domains of syntrophin, DVL3, and PSD-95

Binding of active compounds was validated in an independent assay. ^{15}N-labeled Shank3 PDZ domain was used to record ^{1}H,^{15}N HSQC spectra without and with an eightfold excess of the inhibitor. Shifting amide signals in the superposition of these two spectra indicated binding to the protein for active compounds **34**–**37** (Figure 4 for **34** and **36**, for all compounds, see figure S2 in the Supporting Information).

Finally, binding studies of compounds **34**–**37** were performed using five related PDZ domains, syntrophin, DVL3, PSD-95-1, -2, and -3. For this purpose, HSQC spectra of the five ^{15}N-labeled proteins were recorded with and without ligands. Binding was determined according to the number and distances of shifting amide signals in the overlay of the HSQC spectra (table S3, Supporting Information). While compound **37** only showed shifting signals with the PDZ domains of Shank3 and syntrophin, compounds **35** and **36** additionally displayed binding to DVL3 PDZ and PSD-95-1 PDZ. Compound **34** shifted signals in the ^{1}H,^{15}N HSQC spectra of all tested PDZ domains. The rather unselective nature of tested compounds **34**–**37** is expecta-

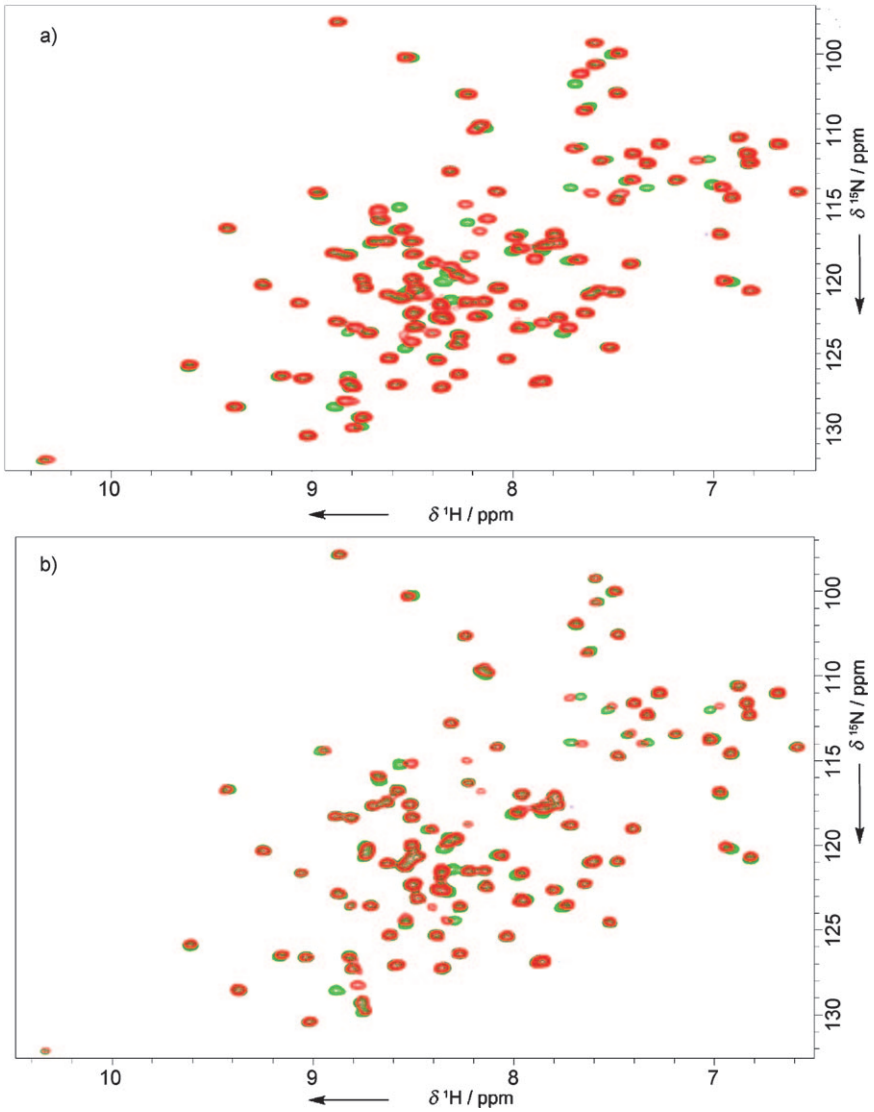

Figure 4. Superposition of ^{1}H, ^{15}N HSQC spectra without ligand (green) and with eightfold excess of ligand (red) for a) compound **34**; b) compound **36**.

ble due to the fact that binding mostly occurred at the carboxylate binding loop present in all PDZ domains.

Shank3 PDZ structure in complex with 36

To elucidate the binding mode of compound **36** toward the Shank3 PDZ domain, we determined the structure of Shank3 PDZ in complex with **36** (PDB: 3O5N). The Shank3 PDZ monomer revealed the reported PDZ fold, with six β-strands forming an antiparallel β-barrel and two α-helices (Figure 5).

As found by a DALI search,[43] the obtained structure displayed the highest degree of structural similarity to rat Shank1 PDZ (PDB: 1Q3O) with an RMSD of 1.2 Å. Furthermore, we

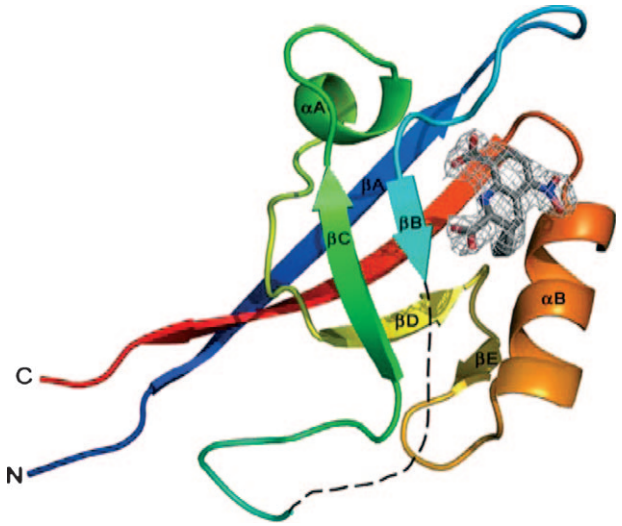

Figure 5. Structure of the Shank3 PDZ domain with bound compound **36**. The Ribbon diagram shows the monomeric structure of the Shank3 PDZ ligand complex with labeled β-strands βA–βF and helices αA and αB. The ligand is colored in dark gray with surrounded $2F_o-F_c$ electron density as mesh in light gray contoured at the 1.0σ level. The dashed line indicates a disordered loop (residues 588–600).

found that both PDZ domains possess similarly extended N-terminal βA and C-terminal βF strands.[33] As for Shank1 PDZ,[33] a similar dimer formation was observed for Shank3 PDZ, with βA strands of each monomer forming an antiparallel β-ladder that causes the N- and C-termini of each PDZ domain to point in opposite directions (figure S3, Supporting Information). The buried dimer interface area was 434 Å^2 or 7.5% of the total surface area of each monomer. Dimer formation in solution was confirmed by size-exclusion chromatography (data not shown). Superposition of the eight molecules per asymmetric unit of Shank3 PDZ showed that they diverge structurally mainly in the more or less defined loop (disordered loop region between residues 588-600 for all molecules) connecting strands βB and βC as well as in the location of their N- and C-termini.

Compound **36** could be clearly identified due to the difference density within the hydrophobic groove between helix αB and strand βB in molecule chain E (figure S4, Supporting Information) at the distal side of the dimer interface. The two carboxylate groups at positions 4 and 6 of **36** formed five hydrogen bonds with a backbone amide of strand βB (L587) and the backbone amides of F583, G584, and F585 of the carboxylate binding loop (Figure 6a). Two additional hydrogen bonds were formed by the nitrogen at position 5 to the carbonyl oxygen of F585 and by the nitro group at position 9 to the side chain of R652. The tetrahydroquinoline was associated with the phenylalanines F583 and F585 by stacking interactions, whereas the cyclopentene ring pointed into the hydrophobic pocket formed by L587, V648, and I651 (Figure 6b). A slightly weaker difference density indicating a partially bound **36**, was also found in the corresponding binding groove of molecule C (figure S4, Supporting Information). The clearly low occupancy, however, did not allow a proper fit and refinement.

Comparison with the very similar rat Shank1 PDZ structure in complex with a hexapeptide[33] (PDB: 1Q3P) revealed that compound **36** evidently mimics the C-terminal leucine of the bound peptide (Figure 7). Superimposition of both bound structures shows that the carboxylate at position 6 and the secondary amine of the inhibitor are close to the carboxylate and nitrogen of leucine. Moreover, the cyclopentene imitates the hydrophobic side chain of the C-terminal amino acid. The second carboxylate at position 4 of **36** is close to the second amide bond of the peptide interacting with the protein backbone (Figure 7). Additional interactions in comparison with the peptide are the stacking interactions with phenylalanines F583 and F585 as well as the interaction of the nitro group at position 9 with R652. These interactions clearly compensate the binding interactions contributed by the other amino acid residues of the bound hexapeptide.

Structure–activity relationship (SAR) studies

All compounds binding to the Shank3 PDZ domain contain a carboxylate group at position R^6 (**34**–**37**, Table S2) together with an adjacent secondary amine at position 5. These two structural features alone, however, are not sufficient for binding as indicated by compound **40**. Tighter binding to the Shank3 PDZ domain is observed for compounds containing a carboxylate or hydroxy functionality at position 6 (**34**–**36**). A pharmacophore containing a carboxylate at position 4, a secondary amine at position 5, and a carboxylate or a hydroxy group at position 6 seems to interact favorably with the carboxylate binding loop and the βB strand, as proven for **36** (Figure 6a). Yet, an additional strong hydrogen bond accepting group such as a nitro functionality at position 8 (R^4 in Table S2; **34** and **36**) or even bridged at position 2 (**35**) is clearly necessary. Loss of this nitro group results in an inactive compound (**39**). A nitro group at R^4 is not sufficient for activity, however, if there is no strong hydrogen bond acceptor such as a carboxylate at position 6 (R^1 in Table S2; **45**). The lower potential of the hydroxy group to form hydrogen bonds relative to carboxylate results in a loss of activity (**43**) if not compensated by a chlorine atom at position 8 (R^3 in Table S2; **34**). The core structure containing the obligatory carboxylate at position 4 (R^6) and the secondary amine at position 5 with a second carboxylate

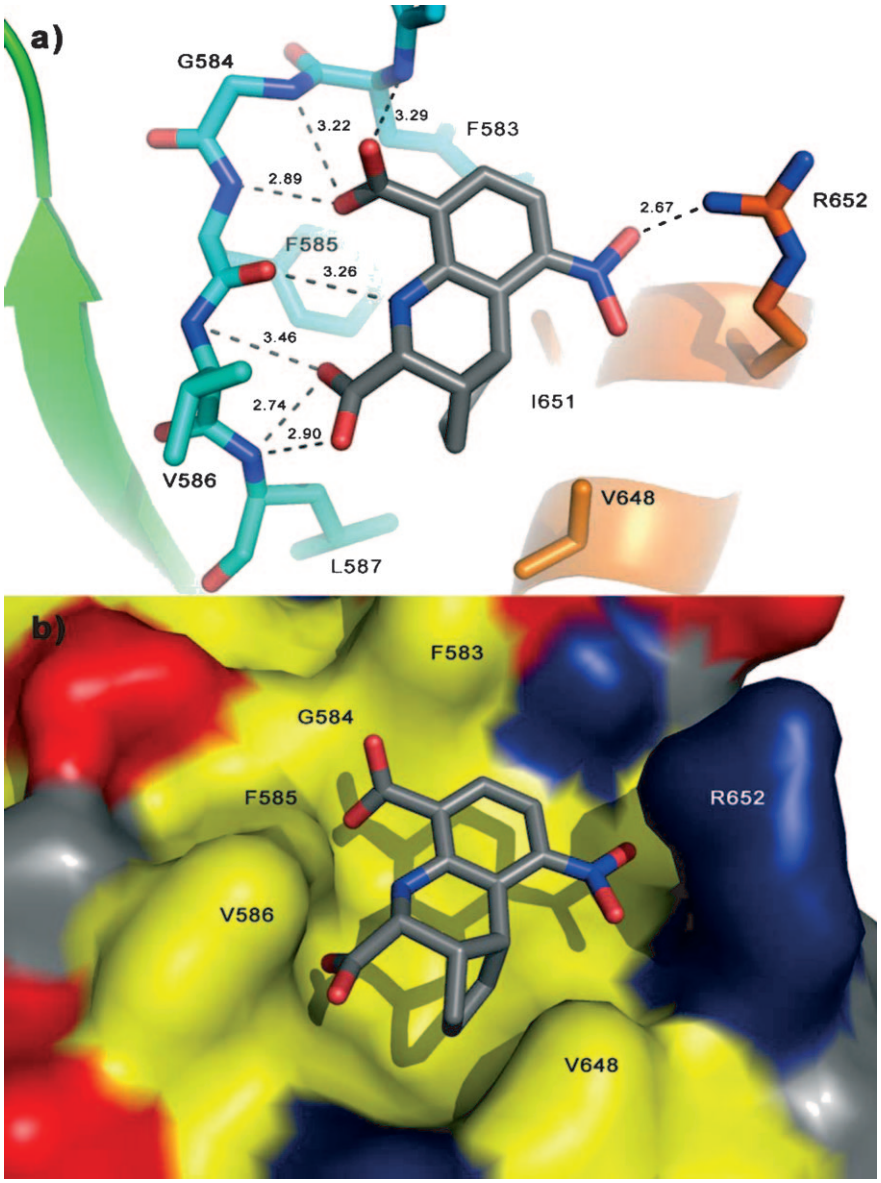

Figure 6. a) Zoom into the binding pocket; hydrogen bonds between **36** and the Shank3 PDZ carboxylate binding loop (light blue) are represented by dashed lines. b) Surface representation of the binding pocket; hydrophobic residues are colored in yellow, while basic and acidic residues are shown in blue and red, respectively.

group at position 8 (R^3) leads to active compound **37**. One of these carboxylates might interact with the carboxylate binding loop; however, the second carboxylate is important as well, as indicated by compounds **38**, **51**, **54**, and **55**. Thus, it cannot be excluded that **37** is located in the binding pocket in a different orientation compared with that observed for **36**. The cyclopentene ring or—in the case of compound **35**—the substituted cyclopentane ring, clearly points into the hydrophobic pocket. The enlargement of the cyclopentene to an indene ring resulted in the inactive compound **46**.

Conclusions

High-affinity peptides binding the Shank3 PDZ domain were developed from a collection of peptides and used to establish a robust fluorescence polarization assay. This tool gave us the possibility to screen the ChemBioNet library for inhibitors. The screening revealed tetrahydroquinoline-4-carboxylates as a new class of inhibitors of the Shank3 PDZ domain. Synthesis and testing of tetrahydroquinoline derivatives indicated that the quinoline scaffold needs the hydrophobic cyclopentyl portion of the molecule, which immerses into the hydrophobic pocket, and the carboxylate group at position 4 together with at least two additional strong hydrogen bond-accepting anchors for binding the Shank3 PDZ domain. Four molecules (**34**–**37**) complying with these requirements displayed K_i values between 10.1 μM and 69.5 μM. All active compounds were validated using NMR spectroscopy. The crystal structure of the Shank3 PDZ domain in complex with inhibitor **36** was analyzed and established the binding mode. Compound **36** is essentially mimicking the C-terminal amino acid of a peptide derived from the native interaction partner GKAP. Most of the active compounds showed activity with a broader spectrum of PDZ domains.

Experimental Section

Chemistry. Solvents and reagents from commercial suppliers in reagent grade were used without further purification, if not otherwise stated. Molecular sieves (Acros Organics, Geel, Belgium) were dried by heating (heat gun) in vacuo for at least 30 min. Reactions were monitored by TLC on precoated silica gel 60 F_{254} aluminum sheets (Merck, Darmstadt, Germany) with UV detection. LC–MS analyses were carried out on an Agilent 1100 system equipped with a reversed-phase column (Nucleosil 100 C_{18}, 5 μm, 2×250 mm, Grom, Herrenberg, Germany); operated with CH_3CN/H_2O mixtures containing 0.1% formic acid, a diode array detector, and a single quadrupole mass spectrometer with electrospray ionization (ESI). ^1H and ^{13}C NMR spectra were measured on a Bruker Avance 300 MHz spectrometer and analyzed using Topspin 2.0.a. HRMS data were obtained on an Agilent 6220 ESI-TOF mass spectrometer. Melting points were recorded using a Büchi Melting Point B545 apparatus (Essen, Germany) and are uncorrected. Microwave irradiation was performed using a Biotage Initiator Microwave Reactor (Uppsala, Sweden). IR spectra were re-

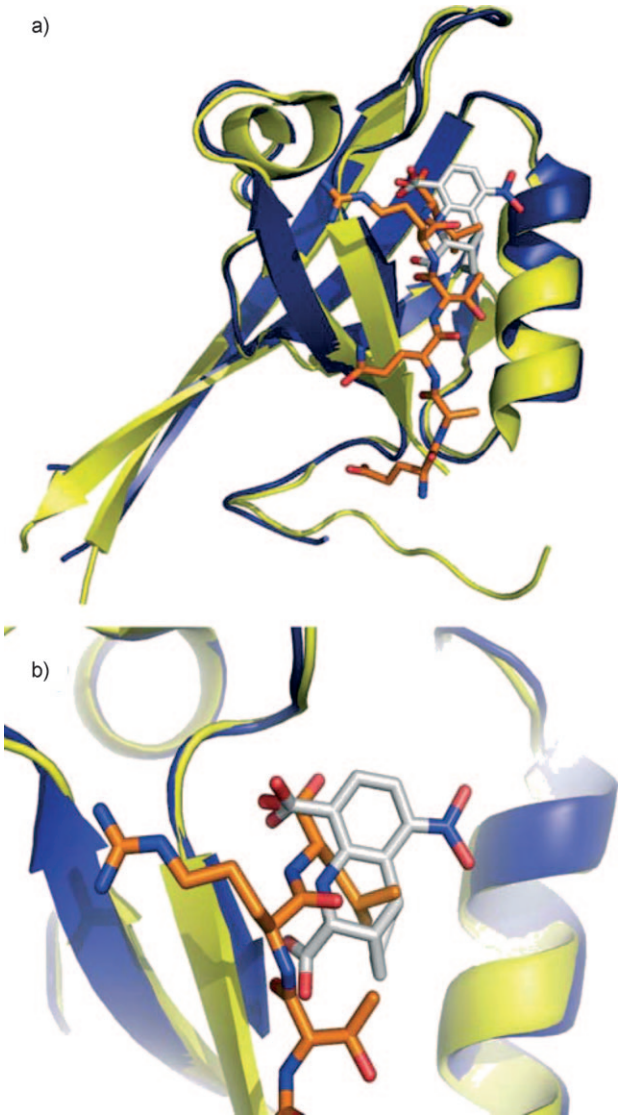

Figure 7. Superposition of rat Shank1 PDZ in yellow with bound hexapeptide (1Q3P) and mouse Shank3 PDZ in blue with bound compound **36**: a) overall view; b) zoom into the binding pocket.

corded using a Vector 22 IR spectrometer (Bruker, Ettlingen, Germany) equipped with a SplitPea-ATR Unit (Harrik, Pleasantville, USA). Peptides were synthesized manually employing plastic syringes equipped with PE filters. The purity of all biologically tested compounds was verified by LC–MS and was at least 98%.

Peptide synthesis. Peptides were synthesized on 2-chlorotrityl chloride resin (Novabiochem, Darmstadt, Germany; 1.3 mmol g^{-1}) using *N*,*N*′-diisopropylcarbodiimide/1-hydroxybenzotriazole (DIC/HOBt) protocols.[44] Fmoc protecting groups were cleaved by treatment with 20% piperidine in DMF twice for 10 min. Following amino acid couplings and Fmoc deprotection, the peptides were acylated using 5(6)-carboxyfluorescein, DIC, and HOBt (5 equiv each). The resin was then shaken in 20% piperidine in DMF for 30 min. Acetylation was done by treatment of the deprotected N-terminus with DMF/Ac_2O/DIPEA (8:1:1) twice for 10 min. Peptides were purified by preparative reversed phase HPLC using CH_3CN-H_2O mixtures containing 0.1% TFA, if necessary (Purity $\geq$ 99%). Analysis was performed using HR-ESI-MS.

CF-QTRL-OH (1): HR-ESI-MS: $[M+H]^+$ calcd for $C_{42}H_{51}N_8O_{13}$: 874.3497, found: 874.3494.

CF-AQTRL-OH (2): HR-ESI-MS: $[M+H]^+$ calcd for $C_{45}H_{56}N_9O_{14}$: 945.3869, found: 945.3868.

CF-EAQTRL-OH (3): HR-ESI-MS: $[M+H]^+$ calcd for $C_{50}H_{63}N_{10}O_{17}$: 1074.4294, found: 1074.4294.

CF-PEAQTRL-OH (4): HR-ESI-MS: $[M+H]^+$ calcd for $C_{55}H_{70}N_{11}O_{18}$: 1171.4822, found: 1171.4819.

CF-HAFTRF-OH (5): HR-ESI-MS: $[M+H]^+$ calcd for $C_{58}H_{62}N_{11}O_{14}$: 1135.4400, found: 1135.4408.

CF-DLQTSI-OH (6): HR-ESI-MS: $[M+H]^+$ calcd for $C_{49}H_{60}N_7O_{18}$: 1033.3917, found: 1033.3912.

Ac-EAQTRL-OH (7): HR-ESI-MS: $[M+H]^+$ calcd for $C_{31}H_{55}N_{10}O_{12}$: 759.3995, found: 759.3995.

General procedure for synthesis of 3a,4,5,9b-tetrahydro-3*H*-cyclopenty[*c*]quinoline-4-carboxylic acid ethyl esters (22–32) and 6,6a,7,11b-tetrahydro-5*H*-indeno[2,1-*c*]quinoline-6-carboxylic acid ethyl ester (33): Aniline derivative **9**–**18** (2.15 mmol) was dissolved in dry CH_3CN (2 mL) containing dried molecular sieves (4 Å, 500 mg), and ethyl glyoxalate (50% solution in toluene, 426 μL, 2.15 mmol) was added. The mixture was stirred for 30 min under nitrogen atmosphere at room temperature. Freshly distilled cyclopentadiene (178 μL, 3.22 mmol) and a solution of 5 mol% $Cu(OTf)_2$ (64 mg, 0.11 mmol) in CH_3CN (0.5 mL) were added. In case of **33**, indene (376 μL, 3.22 mmol) was added. Stirring was continued for 6 h. Subsequently, the molecular sieves were filtered off and washed with EtOAc (15 mL). The combined organic phases were washed with saturated aq. $NaHCO_3$ solution (2×20 mL), followed by extraction of the collected aqueous phases with EtOAc (2× 15 mL). Finally, the combined organic phases were dried over Na_2SO_4 and evaporated to dryness yielding the crude product, which was purified by column chromatography. Data for **9**, **10**, **25**–**32**, **38**, **40**–**46**, **54** and **55** are given in the Supporting Information.

8-Chloro-6-hydroxy-9-nitro-3a,4,5,9b-tetrahydro-3*H*-cyclopenty[*c*]quinoline-4-carboxylic acid ethyl ester (22): Aniline derivative: **9** (405 mg; 2.15 mmol). Column chromatography: *n*-hexane/EtOAc = 2:1. Yellow solid (99 mg, 14%); mp: 179 °C (dec.); ^{1}H NMR (300 MHz, [D_6]DMSO): δ = 6.72 (s, 1H, C*H*, 7), 5.73 (d, *J* = 5.4 Hz, 1H, 1), 5.39 (dd, *J* = 5.4 Hz, *J* = 2.3 Hz, 1H, 1), 5.07 (s, 1H, 5), 4.23–4.07 (m, 4H, CH_2, 2×C*H*, ethyl CH_2, 4, 9b), 3.24 (m, 1H, 3a), 2.36–2.20 (m, 2H, 3), 1.21 ppm (t, *J* = 7.1 Hz, CH_3, ethyl CH_3); ^{13}C NMR (75 MHz, [D_6]DMSO): δ = 170.8 (C, ester C=O), 146.6 (C, aryl C-6), 141.2 (C, aryl C-9), 133.6 (C, aryl C-5a), 132.2 (CH, C-2), 130.6 (CH, C-1), 118.0 (C, aryl C-9b), 112.2 (C, aryl C-8), 111.5 (CH, aryl C-7), 60.8 (CH_2, ethyl CH_2), 54.5 (CH, C-4), 42.5 (CH, C-9b), 39.9 (CH, C-3a), 32.3 (CH_2, C-3), 14.0 (CH_3, ethyl CH_3) ppm; HR-ESI-MS: $[M+H]^+$ calcd for $C_{15}H_{16}ClN_2O_5$: 339.0742, found: 339.0742.

9-Nitro-3a,4,5,9b-tetrahydro-3*H*-cyclopenta[*c*]quinoline-4,6-dicarboxylic acid 4-ethyl ester 6-methyl ester (23): Aniline derivative: **10** (422 mg, 2.15 mmol). Column chromatography: *n*-hexane/EtOAc = 1:1. Orange oil (404 mg, 62%); ^{1}H NMR (300 MHz, [D_6]DMSO): δ = 7.83 (d, *J* = 8.7 Hz, 1H, 7), 7.06 (d, *J* = 8.7 Hz, 1H, 8), 5.73 (bd, *J* = 5.4 Hz, 1H, 2), 5.41 (dd, *J* = 5.4 Hz, *J* = 2.3 Hz, 1H, 1), 4.75 (dd, *J* = 9.1 Hz, *J* = 2.3 Hz, 1H, 9b), 4.36 (d, *J* = 3.8 Hz, 1H, 4), 4.30–4.15 [m, 2H, ethyl CH_2), 3.85 [s, 3H, methyl CH_3), 3.32 (m, 1H, 3a), 2.36–2.19 (m, 2H, 3), 1.25 ppm [t, *J* = 7.1 Hz, 3H, ethyl CH_3)]; ^{13}C NMR (75 MHz, [D_6]DMSO): δ = 170.3 (C, ethyl ester C=O), 166.6 (C, methyl ester C=O), 152.4 (C, aryl C-9), 148.8 (C, aryl C-5a), 132.1 (CH, C-1), 130.8 (CH, C-2), 129.9 (CH, aryl C-7), 118.9 (C, aryl C-9a),

113.3 (C, aryl C-6), 110.7 (CH, aryl C-8), 61.1 (CH_2, ethyl CH_2), 53.7 (CH, C-4), 52.2 (CH_3, methyl CH_3), 42.3 (CH, C-9b), 39.2 (CH, C-3a), 32.3 (CH_2, C-3), 13.9 ppm (CH_3, ethyl CH_3); HR-ESI-MS: $[M+H]^+$ calcd for $C_{17}H_{19}N_2O_6$: 348.1269, found: 348.1272.

3a,4,5,9b-Tetrahydro-3*H*-cyclopenta[*c*]quinoline-4,8-dicarboxylic acid 4-ethyl ester 8-methyl ester (24): Aniline derivative: 4-Amino-benzoic acid methyl ester (**11**, 325 mg, 2.15 mmol). Column chromatography: *n*-hexane/EtOAc = 1:1. Colorless solid (346 mg, 54%); mp: 114 °C (dec.); ^{1}H NMR (300 MHz, [D$_6$]DMSO): δ = 7.57 (d, J = 2.3 Hz, 1H, 9), 7.49 (dd, J = 8.5 Hz, J = 2.3 Hz, 1H, 7), 6.82 (d, J = 8.5 Hz, 1H, 6), 6.31 (s, 1H, 5), 5.84 (dd, J = 5.4 Hz, J = 2.3 Hz, 1H, 1), 5.62 (d, J = 5.4 Hz, 1H, 2), 4.25–4.12 (m, 3H, ethyl CH_2, 4), 4.78 (d, J = 8.7 Hz, 1H, 9b), 3.75 (s, 3H, methyl CH_3), 3.13 (m, 1H, 3a), 2.34–2.15 (m, 2H, 3), 1.23 ppm (t, J = 7.1 Hz, 3H, ethyl CH_3); ^{13}C NMR (75 MHz, [D$_6$]DMSO): δ = 171.0 (C, ethyl ester C=O), 166.1 (C, methyl ester C=O), 149.1 (C, aryl C-5a), 134.7 (CH, C-1), 130.1 (CH, aryl C-9), 129.2 (CH, C-2), 127.6 (CH, aryl C-7), 123.5 (C, aryl C-9a), 117.9 (C, aryl C-8), 114.7 (CH, aryl C-6), 60.5 (CH2, ethyl CH2), 54.3 (CH, C-4), 51.2 (CH_3, methyl CH_3), 44.6 (CH, C-9b), 40.1 (CH, C-3a), 32.0 (CH_2, C-3), 14.0 ppm (CH_3, ethyl CH_3); HR-ESI-MS: $[M+H]^+$ calcd for $C_{17}H_{20}NO_4$: 302.1387, found: 302.1384.

2-Chloro-4-hydroxy-1-nitro-5,6a,7,11b-tetrahydro-6*H*-indeno[2,1-*c*]quinoline-6-carboxylic acid ethyl ester (33): Aniline derivative: **9** (405 mg; 2.15 mmol). Column chromatography: *n*-hexane/EtOAc = 2:1→1:1. Yellow solid (372 mg, 45%); mp: 222 °C (dec.); ^{1}H NMR (300 MHz, [D$_6$]DMSO): δ = 11.00 (s, 1H, O*H*), 7.17 (d, J = 7.0 Hz, 1H, 11), 7.11 (dd, J = 7.0 Hz, J = 7.8 Hz, 1H, 10), 7.05 (ddd, J = 7.4 Hz, J = 7.8 Hz, J = 1.2 Hz, 1H, 9), 6.90 (d, J = 7.4 Hz, 1H, 8), 6.77 (s, 1H, 3), 5.65 (bs, 1H, 5), 4.71 (d, J = 7.3 Hz, 1H, 11b), 4.07 (d, J = 4.9 Hz, J = 1.8 Hz, 1H, 6), 3.69 (q, J = 7.1 Hz, 2H, ethyl CH_2), 3.25 (m, 1H, 6a), 3.09–2.94 (m, 2H, 7), 1.07 ppm (t, J = 7.1 Hz, 3H, ethyl CH_3); ^{13}C NMR (75 MHz, [D$_6$]DMSO): δ = 170.9 (C, non-aromatic C=O), 146.4 (C, aryl C-4), 143.0 and 141.7 (2×C, aryl C-7a and aryl C-11b), 141.4 (C, aryl C-1), 133.8 (C, aryl C-4a), 126.9 (CH, aryl C-10), 126.2 (CH, aryl C-9), 124.8 (CH, aryl C-11), 123.9 (CH, aryl C-8), 115.0 (C, aryl C-11c), 112.1 (C, aryl C-2), 111.8 (CH, aryl C-3), 60.4 (CH_2, ethyl CH_2), 53.7 (CH, C-6), 41.8 (CH, C-11b), 40.7 (CH, C-6a), 32.9 (CH_2, C-7), 13.7 ppm (CH_3, ethyl CH_3); HR-ESI-MS: $[M+H]^+$ calcd for $C_{19}H_{18}ClN_2O_5$: 389.0899, found: 389.0906.

4-(4-Methoxycarbonylphenylcarbamoyl)-3a,4,5,9b-tetrahydro-3*H*-cyclopenta[*c*]quinoline-8-carboxylic acid methyl ester (50): Aniline derivative: 4-Amino-benzoic acid methyl ester (**11**, 325 mg, 2.15 mmol). Column chromatography: *n*-hexane/EtOAc = 1:1. Off-white solid (96 mg, 11%); mp: 244 °C (dec.); ^{1}H NMR (300 MHz, $CDCl_3$): δ = 8.04 (d, J = 8.5 Hz, 1H, 3′), 7.75 (bs, 1H, 9), 7.71 (dd, J = 8.3 Hz, J = 1.3 Hz, 1H, 7), 7.65 (d, J = 8.5 Hz, 1H, 2′), 6.71 (d, J = 8.3 Hz, 1H, 6), 5.94 (bs, 1H, 1), 5.70 (d, J = 5.1 Hz, 1H, 2), 4.28 (d, J = 3.3 Hz, 1H, 4), 4.09 (bd, J = 8.9 Hz, 1H, 9b), 3.91 and 3.87 (2×s, 2×3H, 2×methyl CH_3), 3.24 (m, 1H, 3a), 2.54 (m, 1H, 3_A), 2.32 (m, 1H, 3_B) ppm; ^{13}C NMR (75 MHz, [D$_6$]DMSO): δ = 170.1 (C, amide C=O), 166.2 (C, benzoic acid ester C=O), 165.7 (C, aromatic quinoline carbocylic acid ester C=O), 149.3 (C, aryl C-5a), 143.1 (C, aryl C-1′), 134.4 (CH, C-1), 130.1 (2×CH, aryl C-9 and aryl C-3′), 129.5 (CH, C-2), 127.7 (aryl CH, C-7), 124.1 (C, aryl C-4′), 123.5 (C, aryl C-8), 118.8 (CH, aryl C-2′), 117.8 (C, aryl C-9a), 114.7 (CH, aryl C-6), 56.1 (CH, C-4), 51.8 and 51.2 (2×CH_3, 2×methyl CH_3), 44.7 (CH, C-9b), 40.9 (CH, C-3a), 31.4 ppm (CH_2, C-3); HR-ESI-MS: $[M+H]^+$ calcd for $C_{23}H_{23}N_2O_5$: 407.1601, found: 407.1595.

3a,4,5,9b-Tetrahydro-3*H*-cyclopenta[*c*]quinoline-4,8-dicarboxylic acid 8-methyl ester (51): 24 (400 mg, 1.24 mmol) was suspended in 0.1 M aq. NaOH solution (15 mL). THF was added until a clear solution remained, followed by stirring for 2 h at room temperature. Amberlite® IR-120 hydrogen form was used to neutralize the reaction mixture. The resin was filtered off and washed with H_2O (20 mL). Lyophilization of the filtrate yielded the pure product. Colorless solid (224 mg, 99%); mp: 115 °C (dec.); ^{1}H NMR (300 MHz, [D$_6$]DMSO): δ = 7.55 (s, 1H, 9), 7.47 (dd, J = 8.5 Hz, J = 1.9 Hz, 1H, 7), 6.82 (d, J = 8.5 Hz, 1H, 6), 6.18 (s, 1H, 5), 5.83 (dd, J = 5.0 Hz, J = 2.3 Hz, 1H, 1), 5.62 (d, J = 5.0 Hz, 1H, 2), 4.07 (d, J = 3.5 Hz, 1H, 4), 4.03 (d, J = 9.0 Hz, 1H, 9b), 3.74 (s, 3H, methyl CH_3), 3.16 (m, 1H, 3a), 2.34–2.17 ppm (m, 2H, 3); ^{13}C NMR (75 MHz, [D$_6$]DMSO): δ = 172.5 (C, methyl ester C=O), 166.2 (C, carboxylate C=O), 149.4 (C, aryl C-5a), 134.7 (CH, C-1), 130.1 (CH, aryl C-9), 129.4 (CH, C-2), 127.6 (CH, aryl C-7), 123.7 (C, aryl C-9a), 117.6 (C, aryl C-8), 114.6 (CH, aryl C-6), 54.4 (CH, C-4), 51.2 (CH_3, methyl CH_3), 44.8 (CH, C-9b), 40.2 (CH, C-3a), 32.0 ppm (CH_2, C-3); HR-ESI-MS: $[M+H]^+$ calcd for $C_{15}H_{16}NO_4$: 274.1074, found: 274.1070.

4-Carbamoyl-3a,4,5,9b-tetrahydro-3*H*-cyclopenta[*c*]quinoline-8-carboxylic acid methyl ester (52): To a suspension of **51** (150 mg, 0.55 mmol), Boc_2O (132 mg, 0.60 mmol) and NH_4HCO_3 (260 mg, 3.29 mmol) in dry dioxane (4 mL), pyridine (44 μL, 1.21 mmol) was added under nitrogen atmosphere. After stirring at room temperature for 18 h, the reaction mixture was diluted with EtOAc (15 mL) and washed with H_2O (1×20 mL) and 5% HCl (2×20 mL). The organic phase was dried over Na_2SO_4 and evaporated. Recrystallization from EtOAc and *n*-hexane yielded the title compound. Off-white solid (54 mg, 36%); mp: 228 °C (dec.); ^{1}H NMR (300 MHz, [D$_6$]DMSO): δ = 7.55 (s, 1H, 9), 7.48–7.45 (m, 2H, 7, 1×NH_2), 7,23 (s, 1H, 1×NH_2), 6.78 (d, J = 8.5 Hz, 1H, 6), 6.13 (s, 1H, 5), 5.84 (dd, J = 5.2 Hz, J = 2.2 Hz, 1H, 1), 5.63 (d, J = 5.2 Hz, 1H, 2), 3.99 (d, J = 8.7 Hz, 1H, 9b), 3.93 (d, J = 3.6 Hz, 1H, 4), 3.74 (s, 3H, methyl CH_3), 3.16 (m, 1H, 3a), 2.36–2.26 (m, 1H, 1×3, 2.18–2.10 ppm (m, 1H, 1×3); ^{13}C NMR (75 MHz, [D$_6$]DMSO): δ = 172.3 (C, amide C=O), 166.2 (C, methyl ester C=O), 149.4 (C, aryl C-5a), 134.5 (CH, C-1), 130.1 (CH, aryl C-9), 129.6 (CH, C-2), 127.6 (CH, aryl C-7), 123.6 (C, aryl C-9b), 117.5 (CH, aryl C-6), 114.6 (C, aryl C-8), 54.9 (CH, C-4), 51.2 (CH_3, methyl CH_3), 44.7 (CH, C-9b), 40.8 (CH, C-3a), 32.5 ppm (CH_2, C-3); HR-ESI-MS: $[M+H]^+$ calcd for $C_{15}H_{17}N_2O_3$: 273.1234, found: 273.1228.

4-Hydroxymethyl-3a,4,5,9b-tetrahydro-3*H*-cyclopenta[*c*]quinoline-8-carboxylic acid methyl ester (53): 51 (150 mg, 0.55 mmol) was dissolved in 1,2-dimethoxyethane (7.5 mL), and 4-methylmorpholine (61 μL, 0.55 mmol) and isobutyl chloroformate (75 μL, 0.55 mmol) were added at −15 °C under nitrogen atmosphere. After stirring for 10 min at −15 °C and 10 min at room temperature, the precipitate was filtered off. The filtrate was cooled to −15 °C, and a solution of $NaBH_4$ (31 mg, 0.824 mmol) in H_2O (300 μL) was added. Stirring was continued for 1 min, then H_2O (14 mL) was added. The reaction mixture was extracted with CH_2Cl_2 (3×20 mL). Drying the combined organic phases over Na_2SO_4 and evaporation yielded the crude product, which was purified by column chromatography (EtOAc/*n*-hexane = 4:1). Colorless oil (91 mg, 64%); ^{1}H NMR (300 MHz, [D$_6$]DMSO): δ = 7.53 (s, 1H, 9), 7.46 (dd, J = 8.5 Hz, J = 1.9 Hz, 1H, 7), 6.69 (d, J = 8.5 Hz, 1H, 6), 5.91–5.88 (m, 2H, 5, 1), 5.65 (d, J = 5.2 Hz, 1H, 2), 3.91 (d, J = 8.6 Hz, 1H, 9b), 3.74 (s, 3H, methyl CH_3), 3.52–3.41 (m, 3H, 4, hydroxymethyl CH_2), 2.78 (m, 1H, 3a), 2.31–2.12 ppm (m, 2H, 3); ^{13}C NMR (75 MHz, [D$_6$]DMSO): δ = 166.2 (C, methyl ester C=O), 150.3 (C, aryl C-5a), 134.6 (CH, C-1), 130.4 (CH, aryl C-9), 129.7 (CH, C-2), 127.5 (CH, aryl C-7), 124.1 (C, aryl C-8), 117.3 (C, aryl C-9a), 114.4 (CH, aryl C-6), 63.1 (CH_2, hydroxymethyl CH_2), 53.8 (CH, C-4), 51.1 (CH_3, methyl CH_3), 44.6 (CH, C-9b), 39.5 (CH, C-3a), 30.6 ppm (CH_2, C-3);

HR-ESI-MS: $[M+H]^+$ calcd for $C_{15}H_{18}NO_3$: 260.1281, found: 260.1279.

General procedure for deprotection: The tetrahydroquinoline ester derivative (**23**–**34**, **52**, **53**; 50 mg) was suspended in 0.5 M aq. LiOH solution (5 mL). THF (mixture A) or MeOH (mixture B) was added until a clear solution remained. The mixture was stirred for 2 h at room temperature and then neutralized with Amberlite® IR-120 hydrogen form. The resin was filtered off and washed with H_2O (20 mL). Lyophilization of the filtrate yielded the pure product.

8-Chloro-6-hydroxy-9-nitro-3a,4,5,9b-tetrahydro-3*H*-cyclopenta[*c*]quinoline-4-carboxylic acid (34): 22 (50 mg, 0.15 mmol) was dissolved in mixture B. Yellow solid (45 mg, 99%); mp: 150 °C (dec.); ^{1}H NMR (300 MHz, [D$_6$]DMSO): δ = 11.00 (s, 1H, O*H*), 6.72 (s, 1H, 7), 5.74 (d, J = 5.5 Hz, 1H, 2), 5.40 (dd, J = 5.5 Hz, J = 2.4 Hz, 1H, 1), 4.93 (s, 1H, 5), 4.16 (d, J = 9.2 Hz, 1H, 9b), 4.01 (d, J = 3.5 Hz, 1H, 4), 3.28 (m, 1H, 3a), 2.29 ppm (d, J = 8.9 Hz, 2H, 3); ^{13}C NMR (75 MHz, [D$_6$]DMSO): δ = 172.1 (C, carboxylate C=O), 146.4 (C, aryl C-6), 141.2 (C, aryl C-9), 133.7 (C, aryl C-5a), 132.3 (CH, C-2), 130.4 (CH, C-1), 118.3 (C, aryl C-9a), 112.0 (C, aryl C-8), 111.5 (CH, aryl C-7), 54.5 (CH, C-4), 42.8 (CH, C-9b), 39.9 (CH, C-3a), 32.2 ppm (CH$_2$, C-3); IR (ATR): $\tilde{\nu}$ = 3403, 1715, 1525, 1493, 1363, 1235, 811, 717 cm^{-1}; HR-ESI-MS: $[M+H]^+$ calcd for $C_{13}H_{12}ClN_2O_5$: 311.0429, found: 311.0423.

9-Nitro-3a,4,5,9b-tetrahydro-3*H*-cyclopenta[*c*]quinoline-4,6-dicarboxylic acid (36): 23 (50 mg, 0.14 mmol) was dissolved in mixture B. Brown solid (43 mg, 99%); mp: 202 °C (dec.); ^{1}H NMR (300 MHz, [D$_6$]DMSO): δ = 7.86 (d, J = 8.6 Hz, 1H, 7), 6.92 (d, J = 8.6 Hz, 1H, 8), 5.70 (bd, J = 5.1 Hz, 1H, 2), 5.47 (dd, J = 5.1 Hz, J = 2.1 Hz, 1H, 1), 4.62 (d, J = 9.7 Hz, 1H, 9b), 4.19 (d, J = 3.4 Hz, 1H, 4), 3.40 (m, 1H, 3a), 2.47–2.30 ppm (m, 2H, 3); ^{13}C NMR (75 MHz, [D$_6$]DMSO): δ = 174.0 (C, non-aromatic carboxylate C=O), 170.1 (C, aromatic carboxylate C=O), 154.6 (C, aryl C-9), 151.1 (C, aryl C-5a), 133.0 (CH, C-1), 132.3 (CH, C-2), 131.8 (CH, aryl C-7), 120.7 (C, aryl C-9a), 115.8 (C, aryl C-6), 111.8 (CH, aryl C-8), 55.5 (CH, C-4), 44.6 (CH, C-9b), 41.7 (CH, C-3a), 33.7 ppm (CH$_2$, C-3); IR (ATR): $\tilde{\nu}$ = 3346, 1714, 1524, 1227, 1170, 823, 734, 704 cm^{-1}; HR-ESI-MS: $[M+H]^+$ calcd for $C_{14}H_{13}N_2O_6$: 305.0768, found: 305.0774.

3a,4,5,9b-Tetrahydro-3*H*-cyclopenta[*c*]quinoline-4,8-dicarboxylic acid (37): 24 (50 mg, 0.17 mmol) was dissolved in mixture A. Gray solid (46 mg, 99%); mp: 241 °C (dec.); ^{1}H NMR (300 MHz, [D$_6$]DMSO): δ = 7.49 (s, 1H, 9), 7.41 (d, J = 8.4 Hz, 1H, 7), 6.67 (d, J = 8.7 Hz, 1H, 6), 5.76 (dd, J = 5.9 Hz, J = 2.3 Hz, 1H, 1), 5.60 (d, J = 5.9 Hz, 1H, 2), 3.92 (d, J = 8.8 Hz, 1H, 9b), 3.64 (d, J = 3.6 Hz, 1H, 4), 3.19 (m, 1H, 3a), 2.20 ppm (d, J = 3.6 Hz, 2H, 3); ^{13}C NMR (75 MHz, [D$_6$]DMSO): δ = 173.3 (C, non-aromatic carboxylate C=O), 168.1 (C, aromatic carboxylate C=O), 149.5 (C, aryl C-5a), 135.0 (CH, C-1), 130.3 (CH, aryl C-9), 129.9 (CH, C-2), 127.7 (CH, aryl C-7), 123.8 (C, aryl C-9a), 119.0 (C, aryl C-8), 113.6 (CH, aryl C-6), 56.1 (CH, C-4), 45.5 (CH, C-9b), 41.3 (CH, C-3a), 32.2 ppm (CH$_2$, C-3); IR (ATR): $\tilde{\nu}$ = 3403, 1599, 1270, 1222, 1129, 1108 cm^{-1}; HR-ESI-MS: $[M+H]^+$ calcd for $C_{14}H_{14}NO_4$: 260.0917, found: 260.0914.

3a,4,5,9b-Tetrahydro-3*H*-cyclopenta[*c*]quinoline-4,6-dicarboxylic acid (39): 26 (50 mg, 0.17 mmol) was dissolved in mixture A. Colorless solid (43 mg, 99%); mp: 184 °C (dec.); ^{1}H NMR (300 MHz, [D$_6$]DMSO): δ = 7.56 (d, J = 7.5 Hz, 1H, 7), 7.02 (d, J = 7.2 Hz, 1H, 9), 6.43 (dd, J = 7.5 Hz, J = 7.2 Hz, 1H, 8), 5.69 (dd, J = 5.5 Hz, J = 2.6 Hz, 1H, 1), 5.58 (d, J = 5.5 Hz, 1H, 2), 3.99 (d, J = 9.0 Hz, 1H, 9b), 3.74 [d, J = 3.2 Hz, 1H, 4), 3.22 (m, 1H, 3a), 2.25 ppm (d, J = 9.0 Hz, 2H, 3); ^{13}C NMR (75 MHz, [D$_6$]DMSO): δ = 173.4 (C, non-aromatic carboxylate C=O), 170.3 (C, aromatic carboxylate C=O), 148.2 (C, aryl C-5a), 135.3 (CH, C-1), 131.8 (CH, aryl C-9), 129.6 (CH, C-2), 128.7 (CH, aryl C-7), 126.2 (C, aryl C-9a), 114.7 (CH, aryl C-8), 114.4 (C, aryl C-6), 56.0 (CH, C-4), 46.1 (CH, C-9b), 40.6 (CH, C-3a), 32.7 ppm (CH$_2$, C-3); IR (ATR): $\tilde{\nu}$ = 3370, 1660, 1558, 1433, 1253, 1216, 1147, 740, 691 cm^{-1}; HR-ESI-MS: $[M+H]^+$ calcd for $C_{14}H_{14}NO_4$: 260.0917, found: 260.0919.

1-Chloro-2-(2-nitro-phenylsulfanyl)-2,3,3a,4,5,9b-hexahydro-1*H*-cyclopenta[*c*]quinoline-4,6-dicarboxylic acid (35): 39 (25 mg, 0.10 mmol) was dissolved in dry CH_3CN (2 mL). A solution of 2-nitrobenzenesulfenyl chloride (**63**; 25 mg, 0.12 mmol) in dry CH_3CN (1 mL) was added, followed by stirring for 30 min at room temperature. Finally, the solution was evaporated to dryness yielding the crude product, which was purified by column chromatography ($CHCl_3$/MeOH/AcOH/H_2O = 24:15:3:1). Yellow solid (36 mg, 87%); mp: 171 °C (dec.); ^{1}H NMR (300 MHz, [D$_7$]DMF): δ = 8.37 (s, 1H, 5), 8.19 (dd, J = 7.5 Hz, J = 1.1 Hz, 1H, 3′), 7.83 (dd, J = 7.7 Hz, J = 0.9 Hz, 1H, 7), 7.75–7.76 (m, 2H, 5′ and 6′), 7.59 (d, J = 7.8 Hz, 1H, 9), 7.51 (ddd, J = 7.5 Hz, J = 7.0 Hz, J = 1.9 Hz, 1H, 4′), 6.67 (dd, J = 7.7 Hz, J = 7.8 Hz, 1H, 8), 4.45 (ddd, J = 4.6 Hz, J = 7.6 Hz, J = 7.6 Hz,1H, 2), 4.19 (d, J = 4.1 Hz, 1H, 4), 4.05 (dd, J = 4.6 Hz, J = 4.6 Hz, 1H, 1), 3.66 (dd, J = 8.3 Hz, J = 4.6 Hz, 1H, 9b), 3.31 (m, 1H, 3a), 2.58 (ddd, J = 12.9 Hz, J = 7.6 Hz, J = 5.4 Hz, 1H, 3$_A$), 2.03 ppm (m, 1H, 3$_B$); ^{13}C NMR (75 MHz, [D$_7$]DMF): δ = 172.3 (C, non-aromatic carboxylate C=O), 170.0 (C, aromatic carboxylate C=O), 148.8 (C, aryl C-2′), 148.0 (C, aryl C-5a), 134.1 and 134.1 (2×CH, aryl C-5′ and aryl C-7), 133.6 (C, aryl C-1′), 130.7 (CH, aryl C-7), 130.6 (CH, aryl C-6′),127.1 (CH, aryl C-4′), 125.9 (CH, aryl C-3′), 124.5 (C, aryl C-9a), 116.2 (CH, aryl C-8), 112.4 (C, aryl C-6), 63.2 (CH, C-1), 63.1 (CH, C-2), 54.8 (CH, C-4), 45.8 (CH, C-9b), 39.8 (CH, C-3a), 36.4 ppm (CH$_2$, C-3); IR (ATR): $\tilde{\nu}$ = 3384, 1509, 1246, 1216, 756, 731 cm^{-1}; HR-ESI-MS: $[M+H]^+$ calcd for $C_{20}H_{18}ClN_2O_6S$: 449.0569, found: 449.0561.

Production and purification of recombinant proteins

Shank3 (Q4ACU6, SHANK3_MOUSE, 1805 AA) PDZ domain: Plasmid DNA containing the murine *Shank3* gene was kindly provided by Walter Birchmeier.[28] The PDZ domain-coding sequence corresponding to amino acids (AA) 637–744 was cloned into pLIC-His (carrying the ampicillin resistance (AmpR) gene), kindly provided by Steve Bottomley,[45] resulting in pShank3. The plasmid was transformed into *E. coli* Rosetta (DE3). For large-scale His-Shank3 PDZ (MHHHHHHENLYFQGAAS-Shank3 PDZ) production, a high cell density fermentation (DasGip) on M9-based minimal medium and Overnight Express medium (Novagen) was carried out. Expression for 7 h at 20 °C on minimal medium (fed during induction with ^{15}N-labeled NH_4Cl) yielded ~400 mg L^{-1} culture of His-Shank3 PDZ after one metal-chelating affinity purification (MCP, POROS MC or Ni-NTA), in contrast to ~1000 mg L^{-1} produced at 25 °C for 20 h on Overnight Express medium. A 0.2 mM protein solution (~95% pure) in phosphate buffered saline (PBS), pH 7.2, was used for HTS. For validation of FP hits, pure ^{15}N-labeled tagless PDZ (GAAS-Shank3 PDZ) in 20 mM phosphate buffer (pH 7.2) containing 50 mM NaCl was produced via additional tobacco etch virus (TEV) cleavage and a second MCP. For co-crystallization with ligand, Shank3 PDZ was further purified via gel filtration (Superdex 75). The resulting protein sample was 99% pure.

^{15}N-labeled alpha-1-syntrophin (AAB36398, SNTA1_HUMAN, 505 AA) PDZ Domain: Template plasmid was kindly provided by Maria Macias. The PDZ domain-coding sequence corresponding to AA 84–177 was cloned into pET32a (AmpR) to yield a Trx-His-S-tagged fusion protein. PET32-sPDZ was transformed into BL21(DE3) for expression on M9 minimal medium shaking culture with 0.5 g L^{-1} ^{15}N-labeled NH_4Cl at 30 °C over 4 h with 1 mM IPTG. The fusion protein

was purified via MCP (POROS MC). The PDZ domain was cleaved off by enterokinase and isolated by cation exchange chromatography (POROS HS, 20 mM Tris-HCl, pH 7.4, 50 mM→1000 mM NaCl). The final pure protein (AMADIGS-sPDZ_84–177) was obtained via a second MCP (POROS MC) to remove residual His-tagged fragments. About 40 mg were produced from 1 L M9 minimal medium. The protein was used for NMR in 20 mM phosphate buffer (pH 7.4) containing 50 mM NaCl.

^{15}N-labeled DVL3 (Q92997, DVL3_Human, 716 AA) PDZ domain: For cloning of the DVL3 PDZ domain (AA 243–336), EST clone IMAGp998H1813430Q (ImaGenes, Berlin, Germany) was used as template. The C-terminal cysteine 336 of the domain was exchanged to serine. Through cloning in pET32EK/LIC (AmpR), a coding sequence for a TEV protease cleavage site was introduced. The resulting pDVL3 was transformed into *E. coli* BL21(DE3) Rosetta2. Expression in 2× M9 minimal medium with 0.5 g L^{-1} ^{15}N-labeled NH_4Cl as sole nitrogen source and 1 mM IPTG was done at 25 °C for 40 h with shaking. A yield of 30–40 mg of pure DVL3 was obtained from 1 L culture after MCP, TEV protease cleavage, a second MCP, and gel filtration (Superdex 75). The protein was used for NMR in 20 mM phosphate buffer (pH 7.4) containing 50 mM NaCl.

^{15}N-labeled PSD-95 (P78352, DLG4_HUMAN, 724 AA) PDZ domains: The plasmids (pRSET backbone, AmpR) for His-tagged (MHHHHHPRGS) PDZ1(AA 61–151), PDZ2(AA155–249), and PDZ 3(AA309–401) were kindly provided by Per Jemth.[46] Plasmids were transformed into *E. coli* BL21(DE3) Rosetta2. Expression was done at 25 °C overnight in 2× M9 minimal medium with 0.5 g L^{-1} ^{15}N NH_4Cl as sole nitrogen source and 1 mM IPTG. Purification via MCP (POROS MC) and gel filtration (Superdex 75) yielded 15–30 mg pure protein per liter of medium. For NMR experiments, the His-tagged proteins were used in 20 mM phosphate buffer (pH 7.4) containing 50 mM NaCl.

Fluorescence polarization assays. The assay was carried out on untreated black 384-well microtiter plates (Corning Life Sciences B.V., Schipol–Rijk, Netherlands) in a final volume of 10 μL using 1× PBS (pH 7.2) containing 0.25% Tween as buffer. Measurements were performed on a SAFIRE II microplate reader (Tecan, Crailsheim, Germany) at an excitation wavelength of 470 nm and an emission wavelength of 525 nm. The peptides **1**–**7** were titrated at a concentration of 10 nM against various concentrations (0–100 μM) of His-tagged mShank3 PDZ domain. The measured FP data were analyzed in GraphPad Prism 4 for Windows (GraphPad, La Jolla, CA, USA) by nonlinear regression (curve fit).

Calculation of the *Z′* factor.[37] For the bound state, fluorescence polarization of 500 nM of the His-tagged mShank3 PDZ domain and 10 nM of the fluorescently labeled peptide **3** in PBS (pH 7.2) with 0.25% Tween was measured. The free state was evaluated by adding unlabeled peptide to a final concentration of 10 μM. Mean and standard deviation were calculated to subsequently determine the *Z′* value ($Z' = 0.71$).

IC_{50} determination of hit compounds. His-tagged mShank3 PDZ domain at a concentration of 500 nM and 10 nM of the fluorescently labeled peptide **3** were titrated against various concentrations of the hit compounds (0–500 μM) in 384-well plates. The measured fluorescence polarization (FP) data were analyzed in GraphPad Prism 4 for Windows (GraphPad, La Jolla, CA, USA) by nonlinear regression (curve fit).

Protein NMR spectroscopy. NMR experiments were recorded at 300 K on Bruker DRX600 (equipped with a cryoprobe) and DMX750 spectrometers using triple-resonance probes equipped with self-shielded gradient coils. Spectra were processed by using TOPSPIN 2.0 and analyzed by using SPARKY.[47] NMR samples were prepared using 50 μM ^{15}N-labeled protein in 20 mM sodium phosphate buffer containing 50 mM NaCl at different pH (7.2 for Shank3 and 7.4 for DVL3 and the three PSD95 domains). Compound stock solutions were prepared at 160 mM each in [D_6]DMSO. Individual compounds were added to the ^{15}N-labeled PDZ domain samples at eightfold molar excess. ^{15}N-labeled protein–ligand solutions contained a final concentration of 5% [D_6]DMSO. Reference spectra were acquired in [D_6]DMSO. Ligand binding was detected by measuring ^{1}H,^{15}N HSQC spectra in the absence and presence of compounds. Spectra were acquired with 8 scans and 256 points in the indirect dimension.

Crystallization and X-ray diffraction. Shank3 PDZ was concentrated to 12 mg mL^{-1} in the presence of a fivefold molar excess of **36** (racemic mixture). Crystals of the complex were grown at room temperature using the sitting drop vapor diffusion method in a robotics setup[48] by mixing 0.4 μL of protein solution with 0.4 μL precipitant solution (24% PEG 4000, 14% 2-propanol, 0.15 M NaOAc). Rod-shaped crystals suitable for X-ray diffraction grew within 1–2 weeks. The crystals were cryo-protected for data collection by soaking them for a few seconds in precipitant solution containing 20% (*v*/*v*) PEG 400 and 0.5 mM **36**, and were subsequently frozen in liquid nitrogen. Diffraction data to a resolution of 1.83 Å were collected at 100 K at beamline BL14.1 at the synchrotron-radiation source BESSY,[48] Helmholz-Centrum Berlin, and processed with XDS.[49]

Structure determination and refinement. The diffraction patterns could be indexed in the primitive orthorhombic space group $P2_12_12_1$. Using the structure of the *Rattus norvegicus* Shank1 PDZ domain as a starting model, a molecular replacement solution could be found with the program PHASER,[50] with two molecules of mouse Shank3 PDZ per asymmetric unit. Initial rounds of refinement using the program REFMAC[51] showed unsatisfactorily high crystallographic *R* and free *R* values of 42 and 47%, respectively, and an electron density that did not correspond to a resolution of 1.83 Å. Further refinement, rebuilding, or addition of water molecules could not significantly improve the refinement statistics. Detailed analysis of the X-ray diffraction data in $P2_12_12_1$ by SFCHECK[52] revealed the presence of a 21% pseudo-translation, meaning that a part of the crystal structure has a higher translational symmetry (a shorter translation vector) than the whole structure. The data were reprocessed in the primitive monoclinic space group $P2_1$ and checked for crystallographic twinning. At this point, SFCHECK analysis indicated a high degree of pseudo-merohedral twinning with a twin operator *-h,-k,l* and a twin fraction of 46%. After molecular replacement in space group $P2_1$ with PHASER, a clear solution was found that showed reasonable crystal packing and electron density. The resultant map showing eight molecules per asymmetric unit was readily interpretable. Model building proceeded using the program COOT.[53] Using the "twin refine" option in REFMAC, the structure could be refined to a final crystallographic *R* value of 23.3% and a free *R* value of 28.3%. The crystallographic statistics are given in table S3 (Supporting Information).

Acknowledgements

We thank Dr. Samuel Beligny and Dr. Marco F. Schmidt for support and discussion. The authors gratefully acknowledge support from the DFG (FOR 806 and SFB 765). We thank Sebastian Fiedler,

Martina Leidert, Thao Nguyen, and Natalja Erdmann for excellent technical assistance. The clone for TEV protease production was a generous gift from Gunther Stier. J.R. and U.H. thank the Fonds der Chemischen Industrie for continuous support.

Keywords: fluorescence polarization · high-throughput screening · inhibitors · PDZ domain · protein–protein interactions

[1] J. A. Wells, C. L. McClendon, *Nature* **2007**, *450*, 1001 – 1009.
[2] M. R. Arkin, J. A. Wells, *Nat. Rev. Drug Discovery* **2004**, *3*, 301 – 317.
[3] A. Songyang, A. S. Fanning, C. Fu, J. Xu, S. M. Marfatia, A. H. Chishti, A. Crompton, A. C. Chan, J. M. Anderson, L. C. Cantley, *Science* **1997**, *275*, 73 – 77.
[4] B. J. Hillier, K. S. Christopherson, K. E. Prehoda, D. S. Bredt, W. A. Lim, *Science* **1999**, *284*, 812 – 815.
[5] T. B. C. London, H.-J. Lee, Y. Shao, J. Zheng, *Biochem. Biophys. Res. Commun.* **2004**, *322*, 326 – 332.
[6] D. A. Doyle, A. Lee, J. Lewis, E. Kim, M. Sheng, R. MacKinnon, *Cell* **1996**, *85*, 1067 – 1076.
[7] M. B. Kennedy, *Trends Biochem. Sci.* **1995**, *20*, 350.
[8] P. J. Hajduk, J. R. Huth, S. W. Fesik, *J. Med. Chem.* **2005**, *48*, 2518 – 2525.
[9] D. C. Fry, L. T. Vassilev, *J. Mol. Med.* **2005**, *83*, 955 – 963.
[10] L. You, Z. Xu, C. Punchihewa, D. M. Jablons, N. Fujii, *Mol. Cancer Ther.* **2008**, *7*, 1633 – 1638.
[11] D. Grandy, J. Shan, X. Zhang, S. Rao, S. Akunuru, H. Li, Y. Zhang, I Alpatov, X. A. Zhang, R. A. lang, D.-L. Shi, J. J. Zheng, *J. Biol. Chem.* **2009**, *284*, 16256 – 16263.
[12] A. Bach, N. Stuhr-Hansen, T. S. Thorsen, N. Bork, I. S. Moreira, K. Frydenvang, S. Padrah, S. B. Christensen, K. L. Madsen, H. Weinstein, U. Gether, K. Strømgaard, *Org. Biomol. Chem.* **2010**, *8*, 4281 – 4288.
[13] E. Kim, M. Sheng, *Nat. Rev. Neurosci.* **2004**, *5*, 771 – 781.
[14] W. Feng, M. Zhang, *Nat. Rev. Neurosci.* **2009**, *10*, 87 – 99.
[15] M. Sheng, E. Kim, *J. Cell Sci.* **2000**, *113*, 1851 – 1856.
[16] M. Zhang, W. Wang, *Acc. Chem. Res.* **2003**, *36*, 530 – 538.
[17] S. Naisbitt, E. Kim, J. C. Tu, B. Xiao, C. Sala, J. Valtschanoff, R. J. Weinberg, P. F. Worley, M. Sheng, *Neuron* **1999**, *23*, 569 – 582.
[18] J. C. Tu, B. Xiao, S. Naisbitt, J. P. Yuan, R. S. Petralia, P. Brakeman, A. Doan, V. K. Aakalu, A. A. Lanahan, M. Sheng, *Neuron* **1999**, *23*, 583 – 592.
[19] S. Uchino, H. Wada, S. Honda, Y. Nakamura, Y. Ondo, T. Uchiyama, M. Tsutsumi, E. Suzuki, T. Hirasawa, S. Kohsaka, *J. Neurochem.* **2006**, *97*, 1203 – 1214.
[20] H. Zitzer, D. Richter, H.-J. Kreienkamp, *J. Biol. Chem.* **1999**, *274*, 18153 – 18156.
[21] H.-J. Kreienkamp, H. Zitzer, D. Richter, *J. Physiol. (Paris)* **2000**, *94*, 193 – 198.
[22] M. K. Baron, T. M. Boeckers, B. Vaida, S. Faham, M. Gingery, M. R. Sawaya, D. Salyer, E. D. Gundelfinger, J. U. Bowie, *Science* **2006**, *311*, 531 – 535.
[23] C. Sala, V. Piech, N. R. Wilson, M. Passafaro, G. Liu, M. Sheng, *Neuron* **2001**, *31*, 115 – 130.
[24] B. Qualmann, T. M. Boeckers, M. Jeromin, E. D. Gundelfinger, M. M. Kessel, *J. Neurosci.* **2004**, *24*, 2481 – 2495.
[25] C. M. Durand et al., *Nat. Genet.* **2007**, *39*, 25 – 27.
[26] T. Bourgeron, *Curr. Opin. Neurobiol.* **2009**, *19*, 231 – 234.
[27] S.-H. Shi, T. Cheng, L. Y. Jan, Y.-N. Jan, *Proc. Natl. Acad. Sci. USA* **2004**, *101*, 13346 – 13351.
[28] G. Schuetz, M. Rosário, J. Grimm, T. M. Boeckers, E. D. Gundelfinger, W. Birchmeier, *J. Cell Biol.* **2004**, *167*, 945 – 952.
[29] C. Borghouts, C. Kunz, B. Groner, *J. Pept. Sci.* **2005**, *11*, 713 – 726.
[30] D. Derossi, G. Chassaing, A. Prochiantz, *Trends Cell Biol.* **1998**, *8*, 84 – 87.
[31] M. Lisurek, B. Rupp, J. Wichard, M. Neuenschwandner, J. P. von Kries, R. Frank, J. Rademann, R. Kühne, *Mol. Diversity* **2010**, *14*, 401 – 408.
[32] J. Schultz, R. R. Copley, T. Doerks, C. P. Ponting, P. Bork, *Nucleic Acids Res.* **2000**, *28*, 231 – 234.
[33] Y. J. Im, J. H. Lee, S. H. Park, S. J. Park, S. H. Roh, G. B. Kang, E. Kim, S. H. Eom, *J. Biol. Chem.* **2003**, *278*, 48099 – 48104.
[34] F. W. Studier, *Protein Expression Purif.* **2005**, *41*, 207 – 234.
[35] M. A. Stiffler, J. C. Chen, V. P. Grantcharova, Y. Lei, D. Fuchs, J. E. Allen, L. Zaslavskaia, G. MacBeath, *Science* **2007**, *317*, 364 – 369.
[36] Z. Nikolovska-Coleska, R. Wang, X. Fang, H. Pan, Y. Tomita, P. Li, P. P. Roller, K. Krajewski, N. G. Saito, J. A. Stuckey, S. Wang, *Anal. Biochem.* **2004**, *332*, 261 – 273.
[37] J.-H. Zhang, T. D. Y. Chung, K. R. Oldenburg, *J. Biomol. Screening* **1999**, *4*, 67 – 73.
[38] S. Hermitage, J. A. K. Howard, D. Jay, R. G. Pritchard, M. R. Probert, A. Whiting, *Org. Biomol. Chem.* **2004**, *2*, 2451 – 2460.
[39] W. Borsche, *Ber. Dtsch. Chem. Ges.* **1917**, *50*, 1339 – 1355.
[40] W. Heyne, L. Walter (VEB Farbenfabrik Wolfen), GB911 809, **1962**.
[41] S. Kobayashi, H. Ishitani, S. Nagayama, *Synthesis* **1995**, 1195 – 1202.
[42] V. Lucchini, M. Prato, G. Scorrano, P. Tecilla, *J. Org. Chem.* **1988**, *53*, 2251 – 2258.
[43] L. Holm, S. Kaariainen, P. Rosenstrom, A. Schenkel, *Bioinformatics* **2008**, *24*, 2780 – 2781.
[44] *Fmoc Solid-Phase Peptide Synthesis* (Eds.: W. C. Chan, P. D. White), Oxford University Press, Oxford **2000**.
[45] L. D. Cabrita, W. Dai, S. P. Bottomley, *BMC Biotechnol.* **2006**, *6*, 12.
[46] A. Bach, C. N. Chi, T. B. Olsen, S. W. Pedersen, M U. Røder, G. F. Pang, R. P. Clausen, P. Jemth, K. Strømgaard, *J. Med. Chem.* **2008**, *51*, 6450 – 6459.
[47] T. D. Goddard, D. G. Kneller, SPARKY 3, University of California, San Francisco, **2003**.
[48] U. Heinemann, K. Büssow, U. Mueller, P. Umbach, *Acc. Chem. Res.* **2003**, *36*, 157 – 163.
[49] W. Kabsch, *J. Appl. Crystallogr.* **1993**, *26*, 795 – 800.
[50] A. J. McCoy, R. W. Grosse-Kunstleve, P. D. Adams, M. D. Winn, L. C. Storoni, R. J. Read, *J. Appl. Crystallogr.* **2007**, *40*, 658 – 674.
[51] G. N. Murshudov, A. A. Vagin, E. J. Dodson, *Acta Crystallogr. Sect. D* **1997**, *53*, 240 – 255.
[52] A. A. Vaguine, J. Richelle, S. J. Wodak, *Acta Crystallogr. Sect. D* **1999**, *55*, 191 – 205.
[53] P. Emsley, K. Cowtan, *Acta Crystallogr. Sect. D* **2004**, *60*, 2126 – 2132.

Received: February 15, 2011
Published online on May 27, 2011

